Metal-phosphorus-imidazole synergistic complexes for enhancing latency and fire safety in single-component epoxy resins

Jingsheng Wang[a], Jun Wang[a], Shuang Yang[b,*], Renxin Xu[a], Guoping Ding[b], Wei Liu[c], Jiuxiao Sun[d,*], Kaiwen Chen[a], Liu Duan[a], Gen Zhou[e], Xian Liu[e], Siqi Huo[f]

[a] *School of Materials Science and Engineering, Wuhan University of Technology, Wuhan 430070, China*

[b] *School of Mechanical and Electronic Engineering, Wuhan University of Technology, Wuhan 430070, China*

[c] *Bamstone New Material Technology Co., Ltd, Wuhan 430070, China*

[d] *School of Materials Science and Engineering, Wuhan Textile University, Wuhan 430070, China*

[e] *Wuhan East Lake High Technology Group Co., Ltd, Wuhan 430070, China*

[f] *School of Engineering, Centre for Future Materials, University of Southern Queensland, Springfield 4300, Australia*

** Corresponding author:*

Email: ysfrp@whut.edu.cn (S. Yang)

Email: 2017002@wtu.edu.cn (J. Sun)

Abstract: In response to the increasing need for fire-resistant single-component epoxy resin (EP) systems, this research introduces five metal-based phosphorus/imidazole-containing complexes (M-DA) as latent curing agents. These complexes, synthesized by coordinating Fe^{3+}, Co^{2+}, Ni^{2+}, Cu^{2+}, or Zn^{2+} into a phosphorus-containing imidazole derivative (DA), were designed to improve flame retardancy, smoke suppression, and latency of single-component EPs. EP/M-DA mixtures exhibited prolonged shelf life and rapid gel times at moderate temperatures, with latency improvements following the

trend: $Cu^{2+} > Ni^{2+} > Co^{2+} > Zn^{2+} > Fe^{3+}$. Notably, EP/Cu-DA achieved a storage life of 43 days. In addition, it demonstrated improved thermal stability as well as superior mechanical strength and toughness. All EP/M-DA thermosets achieved a UL-94 V-0 rating and high limiting oxygen index (LOI) values exceeding 29.0%, with EP/Cu-DA showing the highest LOI of 37.5%. EP/Cu-DA also achieved significant reductions (46.5% and 21.1%) in peak heat release rate and total smoke production, highlighting its superior flame retardancy and smoke suppression. These improvements were attributed to synergistic effects between transition metal ions and phosphorus, which promote condensed-phase carbonization and gaseous-phase combustion inhibition. Among the single-component EPs, EP/Cu-DA exhibited the best combination of latency, mechanical strength, fire safety, and smoke suppression, providing a promising strategy for developing high-performance single-component EPs.

Keywords: Single-component epoxy resin; metal-phosphorus synergism; fire safety; smoke suppression.

1. Introduction

The extensive application of epoxy resins (EPs) across diverse high-performance fields, including aerospace, electronics, and automotive industries, necessitates the development of materials with enhanced fire safety [1-3]. While common EPs are highly valued for their excellent mechanical properties, thermal stability, and adhesion, their inherent flammability and the generation of dense smoke during combustion pose significant safety risks [4-6]. These issues are particularly critical in confined or safety-critical environments, making it imperative to develop EP systems with satisfactory

flame retardancy and smoke suppression capabilities without compromising material performance [7, 8]. Single-component EPs, as promising alternatives to traditional two-component systems, offer improved user convenience by eliminating the need for on-site mixing, minimizing waste, and enhancing processing efficiency [9, 10]. The cornerstone of single-component EP technology lies in the design of latent curing agents, which remain stable during storage and activate under specific thermal conditions to initiate robust curing [11]. However, achieving both intrinsic flame retardancy and effective smoke suppression while maintaining adequate latency remains a formidable challenge for single-component EP systems [12-14].

Among the numerous curing agents for epoxy resins, imidazole can initiate anionic polymerization, offering rapid curing at moderate temperatures. However, conventional imidazoles exhibit poor latency at room temperature, often lasting less than one day, making them unsuitable for single-component epoxy resin systems. Phosphorus (P)-containing imidazole derivatives have emerged as promising flame-retardant latent curing agents for EPs [15-18]. These compounds leverage the dual functionalities of P-based groups: 1) the ability to covalently bond within the crosslinked resin network, imparting intrinsic flame retardancy, and 2) the electronic and spatial characteristics of P-substituents, which diminish the reactivity of imidazole, thereby enhancing latent curing behavior [13, 14, 19-21]. For example, our previous study reported a phosphorus-containing imidazole hardener (DA), which notably enhanced the fire safety of EPs, achieving a LOI of 37.2% and a UL-94 V-0 rating [22]. Nevertheless, the shelf life of DA remained inadequate for practical use, and the combustion of EP/DA

resulted in substantial smoke generation due to the dominance of gas-phase flame-retardant mechanisms associated with the low oxidation state of phosphorus.

To address these limitations, incorporating transition metal ions into P-containing imidazoles has been identified as an effective approach [23, 24]. Transition metals play a critical role in enhancing flame resistance and reducing smoke production through their catalytic and synergistic effects [25, 26]. Specifically, during combustion, metal ions can accelerate the dehydration and aromatization processes within the polymer matrix, thereby enhancing the formation of char [27-29]. This compact and heat-resistant char serves as a protective physical shield, restricting the emission of flammable gases and reducing the heat and mass flow between the flame zone and underlying matrix. In the gaseous phase, transition metal ions exhibit significant catalytic oxidation capabilities, facilitating the full combustion of smoke particulates and converting toxic gases like carbon monoxide into the less hazardous carbon dioxide [24, 25, 30]. This not only reduces the amount of visible smoke but also lowers the toxicity of combustion products, thereby enhancing the overall fire safety of the system. Furthermore, by coordinating with tertiary amines, transition metal ions suppress the nucleophilicity of the imidazole group, which effectively prolongs the latency of hardener. [31-34]. In a prior study, we developed a copper-coordinated phosphorus-based imidazole complex (Cu-DA) through the reaction of DA with $CuCl_2$. The resultant EP/Cu-DA system demonstrated significantly improved latency, maintaining a storage life for 43 days and rapidly curing when exposed to higher temperatures. Importantly, the system exhibited superior flame retardancy (LOI of 37.8%, UL-94 V-

0 rating) and reduced smoke generation, resulting from the combined synergistic effects of Cu^{2+} and phosphorus species [19], which enhanced char formation and suppressed volatile emissions.

Encouraged by these promising results, this work extended the strategy to investigate the effects of incorporating various transition metal ions (Fe^{3+}, Co^{2+}, Ni^{2+}, Cu^{2+}, and Zn^{2+}) into P-containing imidazoles. The study systematically evaluated the influence of these five metal-based phosphorus/imidazole-containing complexes on key performance metrics, including latency, thermal stability, mechanical properties, flame retardancy, and smoke suppression of single-component EP systems. By elucidating the synergistic effects of different metal ions and phosphorus-containing imidazoles, the findings aim to establish a versatile framework for designing advanced single-component EPs that combine long-term latency, efficient flame retardancy, and superior smoke suppression, addressing critical safety and performance requirements for industrial applications.

2. Experiment section

2.1. Synthesis of phosphorus-containing imidazole (DA)

DA was synthesized following the methodology outlined in our previous research [22], and its molecular structure is shown in Fig. 1a.

2.2. Synthesis of transition metal-based phosphorus/imidazole-containing complexes (M-DA complexes)

The synthesis of five M-DA complexes was performed following a standard protocol. In a 150 mL three-neck flask equipped with a stirrer and a dropping funnel,

ferric chloride (0.03 mol, 4.9 g) and 60 mL of ethanol were added and stirred until a homogeneous solution was obtained. The mixture was then heated to 60 °C. Separately, DA (0.03 mol, 9.8 g) was dissolved in 40 mL of ethanol and transferred to the dropping funnel. Over the course of 1 hour, this solution was slowly added dropwise to the flask. After the addition was complete, the reaction was allowed to proceed at 60 °C for an additional 6 hours. Subsequently, the mixture was cooled to room temperature. A precipitate formed during the process, which was collected by filtration, washed thoroughly three times with ethanol to remove impurities, and vacuum-dried to obtain a brownish-red solid identified as Fe-DA.

Similarly, Co-DA, Ni-DA, Cu-DA, and Zn-DA were synthesized by replacing ferric chloride with cobalt chloride hexahydrate, nickel chloride, copper chloride, and zinc chloride, respectively, while maintaining the same reaction conditions.

2.3. Preparation of EP thermosets

The compositions of the EP thermosets are detailed in Table 1. EP/DA and EP/M-DA thermosets (EP/Fe-DA, EP/Co-DA, EP/Ni-DA, EP/Cu-DA, and EP/Zn-DA) were prepared using DA and the corresponding M-DA complexes as curing agents, respectively. To explore the effects of transition metal ions in M-DA on the comprehensive properties of EP/M-DA systems, a consistent DA content of 16 g per 100 g of epoxy resin was maintained across the EP/DA and EP/M-DA formulations. This maintained uniform phosphorus levels, eliminating interference from varying DA or phosphorus content. For EP/DA, the fabrication process involved mixing E51 with DA at 50 °C while stirring to ensure uniform dispersion. The mixture was then degassed

in a vacuum desiccator to remove trapped air and subsequently transferred into a preheated mold. The curing schedule consisted of sequential heating at 80 °C for 2 hours, 130 °C for 2 hours, and 180 °C for 1 hour.

For EP/M-DA thermosets, EP was mixed with the M-DA complexes at 80 °C and stirred for 30 minutes to achieve homogeneity. The degassed mixtures were then transferred to molds and cured following the same procedure as EP/DA.

Table 1. Compositions of EP samples.

Samples	EP (g)	DA (g)	M-DA (g)	Posphorus content (wt%)	Metal content (wt%)
EP/DA	100	16.0	/	1.31	/
EP/Fe-DA	100	/	17.3	1.30	0.39
EP/Co-DA	100	/	17.6	1.30	0.62
EP/Ni-DA	100	/	17.6	1.30	0.61
EP/Cu-DA	100	/	17.6	1.29	0.66
EP/Zn-DA	100	/	17.6	1.29	0.68

2.4. Materials and characterization

Please see the Supporting Information.

3. Results and discussion

3.1. Characterizations of phosphorus/imidazole-containing complexes

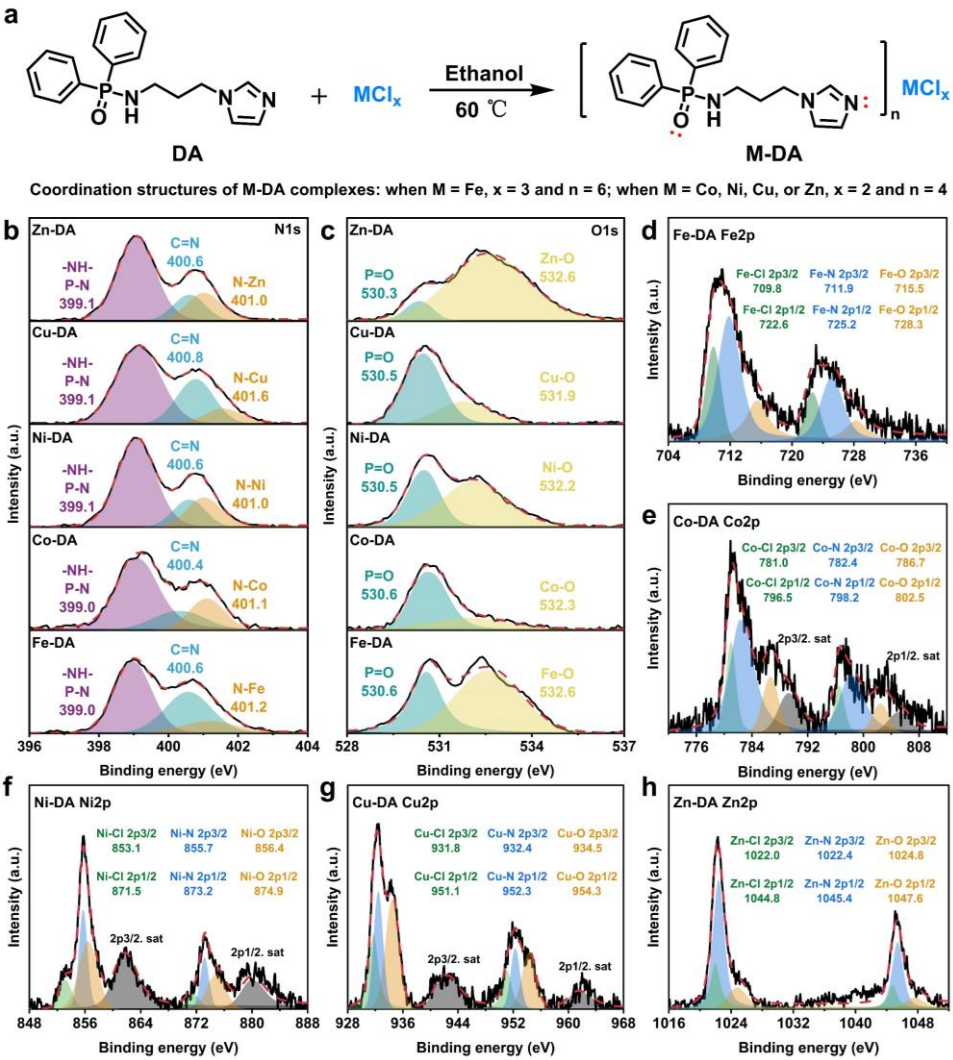

Fig. 1. (a) Synthesis route of M-DA complexes; high-resolution XPS spectra of M-DA complexes: (b) N1s, (c) O1s, (d) Fe2p for Fe-DA, (e) Co2p for Co-DA, (f) Ni2p for Ni-DA, (g) Cu2p for Cu-DA, and (h) Zn2p for Zn-DA.

The chemical structures of M-DA complexes were systematically characterized using Fourier-transform infrared (FTIR) spectroscopy, X-ray photoelectron spectroscopy (XPS), elemental analysis (EA), and inductively coupled plasma optical emission spectrometry (ICP-OES), as summarized in Fig. S1, Fig. 1, and Table S1. In the FTIR spectrum of DA (see Fig. S1a), characteristic absorption peaks associated with the benzene ring were observed at 1593, 833, and 729 cm^{-1} [19, 20]. Peaks at 3217,

1650, and 1139 cm^{-1} belonged to N-H, C=N, and P=O groups, respectively [13, 14, 19]. Upon coordination with transition metal chlorides, the C=N and P=O absorption peaks underwent varying degrees of redshift in the M-DA complexes, indicating the interaction between DA and metal ions [33, 35]. For example, the C=N peak around 1650 cm^{-1} shifted to 1638 cm^{-1} for Fe-DA and to 1632 cm^{-1} for other M-DA complexes. Additional peaks at 597 and 430 cm^{-1}, corresponding to Metal-O and Metal-N bonds [35-37], respectively, further supported the coordination between nitrogen atoms in imidazole groups, oxygen atoms in phosphate groups, and transition metal ions.

XPS analysis provided complementary evidence for the coordination between DA and transition metal ions. As depicted in Fig. S1b, the full-scan spectra of the M-DA complexes showed the detection of elements including carbon, nitrogen, oxygen, phosphorus, and chlorine, along with the respective metal ions. The high-resolution N1s spectra exhibited two key peaks around 399.1 eV and 400.5 eV, associated with the -NH-/P-N and C=N bonding environments, respectively (see Fig. 1b) [38]. A distinct peak around 401.2 eV was associated with the formation of coordination bonds between nitrogen atoms and transition metal ions [35]. In the O1s region, the peak around 530.4 eV corresponded to O=P groups, whereas the peak at around 532.5 eV indicated the interaction between oxygen atoms and transition metal ions (see Fig. 1c) [13, 14]. Furthermore, high-resolution spectra for Fe2p, Co2p, Ni2p, Cu2p, and Zn2p showed characteristic peaks associated with Metal-Cl, Metal-N, and Metal-O bonds, further confirming successful coordination between the DA ligand and transition metal ions (Fe^{3+}, Co^{2+}, Ni^{2+}, Cu^{2+}, and Zn^{2+}) (see Fig. 1d-h) [30, 35]. In Table S1, EA and ICP-

OES measurements revealed that Fe-DA contained 8.63 wt% phosphorus and 2.62 wt% iron, which aligns with a DA to $FeCl_3$ molar ratio of approximately 6:1. Similarly, the molar ratios of DA to transition metal chlorides in Co-DA, Ni-DA, Cu-DA, and Zn-DA were calculated to be approximately 4:1. The findings supported the successful formation of the M-DA complexes: Fe-DA was determined to consist of one $FeCl_3$ molecule complexed with six DA ligands, while Co-DA, Ni-DA, Cu-DA, and Zn-DA were composed of one transition metal halide molecule complexed with four DA ligands. These distinct stoichiometric differences reflect the varied coordination behaviors of different metal ions, which may influence their contributions to latency in the final epoxy systems.

3.2. Latent curing behaviors

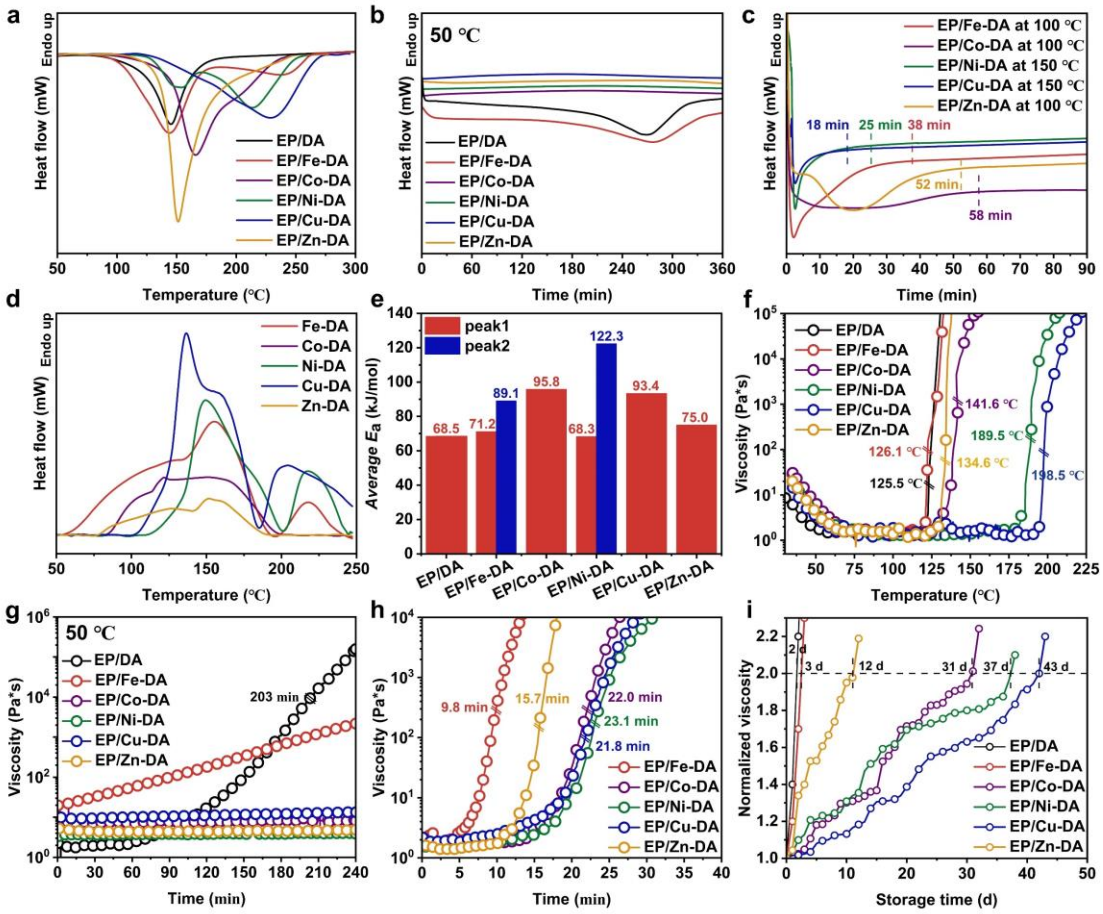

Fig. 2. (a) Non-isothermal DSC curves of EP mixtures; isothermal DSC curves of EP mixtures at (b) 50 °C and (c) 100 or 150 °C; (d) non-isothermal DSC curves of M-DA complexes; (e) apparent activation energies; (f) viscosity versus temperature curves; viscosity versus time curves at (g) 50 °C and (h) 100 or 150 °C (100 °C for M = Fe, Co, and Zn; 150 °C for M = Ni and Cu); and (i) Viscosity curves of EP mixtures over time during storage at 25 °C, normalized for comparison.

The curing characteristics of the EP mixtures were investigated through non-isothermal differential scanning calorimetry (DSC), with findings summarized in Fig. 2a and Table S2. The EP/DA mixture demonstrated a single, symmetric exothermic peak at 145.3 °C, corresponding to the addition and etherification reactions involving the epoxy group and the secondary amine as well as the imidazole ring of DA [7, 22].

Incorporating transition metal ions significantly altered the curing profiles of EP/M-DA mixtures. The DSC curves displayed either two distinct peaks or an asymmetric profile, reflecting the complex curing behaviors induced by the metal-ligand interactions. The peak curing temperatures (T_ps) shifted to 143.7 °C (EP/Fe-DA), 166.1 °C (EP/Co-DA), 154.3 °C (EP/Ni-DA), 229.1 °C (EP/Cu-DA), and 151.3 °C (EP/Zn-DA), indicating the varied influence of different metal ions on the reactivity of DA. Interestingly, EP/Fe-DA and EP/Ni-DA mixtures displayed a second exothermic peak at 237.1 °C and 213.0 °C, respectively. The elevated T_ps of EP/M-DA mixtures, compared with EP/DA, demonstrated the inhibitory effect of transition metal complexation on DA reactivity, a critical feature contributing to the enhanced thermal latency of these curing systems. Further assessment of curing behaviors in the EP mixtures was conducted using isothermal DSC. At 50 °C, the EP/DA mixture showed an exothermic reaction after 200 minutes, signaling the onset of the curing process. By contrast, EP/Fe-DA showed a slightly delayed exothermic response due to the moderate inhibitory effects of Fe^{3+} on DA. Notably, other EP/M-DA mixtures exhibited an absence of detectable exothermic peaks even after 360 minutes, indicating a markedly reduced curing reactivity and significantly improved thermal latency (see Fig. 2b). When subjected to elevated temperatures, the EP/M-DA mixtures transitioned swiftly into the curing phase. EP/Fe-DA, EP/Co-DA and EP/Zn-DA reached full cure within 60 minutes at 100 °C, while EP/Ni-DA and EP/Cu-DA completed curing within 30 minutes at 150 °C (see Fig. 2c). The results suggest that M-DA complexes are stable and inactive at low temperatures, but they trigger rapid curing of epoxy resins at elevated temperatures, demonstrating

their suitability as efficient latent curing agents for single-component epoxy systems.

To investigate the curing behavior of M-DA in EP, non-isothermal DSC measurements were carried out on the M-DA complexes (see Fig. 2d). The DSC curves for M-DA complexes revealed a distinct endothermic transition within the 50-250 °C range, attributed to the stepwise decomposition of the M-DA complexes. This decomposition behavior, previously confirmed in studies of Cu-DA complexes [19], aligns closely with the curing temperature range of EP/M-DA mixtures, indicating a direct relationship between complex dissociation and curing initiation. For instance, the peak decomposition temperatures (T_ds) of Ni-DA were identified at 149.4 °C and 217.4 °C, which corresponded well with the curing peaks of EP/Ni-DA at 154.3 °C and 213.0 °C. The presence of multiple or overlapping peaks in the DSC profiles of M-DA complexes is likely due to a stepwise dissociation process, wherein the sequential breakdown of coordination bonds between the DA ligands and the metal ions occurs at varying temperatures [39]. Initially, complexes with a greater number of ligands dissociate at lower temperatures. As dissociation proceeds and ligand numbers decrease, metal-ligand interactions strengthen, requiring higher energies for further dissociation [40]. As ligands gradually dissociate, the curing reaction is sequentially activated, which provides a controllable mechanism to tune the reactivity and latency of these single-component epoxy systems. Building on the preceding analysis, the curing mechanism of the EP/M-DA mixture can be described as a stepwise dissociation of DA from the M-DA complex triggered by elevated temperatures. This dissociation initiates anionic polymerization between the epoxy groups and the imidazole rings, while

nucleophilic addition occurs between the epoxy groups and the secondary amine groups in DA. The reaction proceeds with etherification and propagation, ultimately leading to the formation of a crosslinked epoxy network. These findings suggest that the curing process in EP/M-DA systems is closely coupled with the stepwise dissociation of M-DA complexes. This coupling links the thermal stability of M-DA complexes directly to the curing reactivity and latency of EP/M-DA systems, offering a pathway for fine-tuning curing profiles through metal-ligand design.

To elucidate differences in curing activity among M-DA complexes, the curing kinetics of EP mixtures were evaluated using the Kissinger, Crane, and Flynn-Wall-Ozawa models. Plots of $\ln(\beta/T_p^2)$ versus $1/T_p$ and $\ln(\beta)$ versus $1/T_p$ are shown in Fig. S2g and h [41, 42]. Kinetic parameters from these models are presented in Table S3, with average activation energies (E_as) depicted in Fig. 2e. E_a values, which serve as indicators of curing difficulty [12, 42], showed that the first curing peak of EP/Fe-DA had an E_a of 71.2 kJ/mol, similar to 67.0 kJ/mol for EP/DA, while the second peak reached 89.1 kJ/mol. The difference in E_a between the two curing peaks for EP/Fe-DA may stem from the stepwise dissociation of Fe-DA. At high coordination numbers, the metal-ligand interactions are relatively weak, which facilitates DA dissociation and initiates curing at lower temperatures, resulting in a lower E_a. With partial dissociation, the coordination environment changes, strengthening the interaction between metal and remaining ligands, and requiring higher energy for further dissociation [43]. A similar trend was observed in the EP/Ni-DA system, though with some differences. The curing exotherm of EP/Fe-DA was concentrated in the first curing peak, whereas the main

curing for EP/Ni-DA occurred at the second peak (see Fig. 2b and Table S2). This suggested that Ni-DA dissociation predominantly took place in a later decomposition stage, thereby indicating that the curing reactivity of Ni-DA is primarily governed by the subsequent decomposition of Ni-DA. The second curing peak of EP/Ni-DA exhibited the highest E_a of 122.3 kJ/mol among all EP mixtures. The E_as of EP/Co-DA, EP/Cu-DA, and EP/Zn-DA measured 95.8, 93.4, and 75.8 kJ/mol, respectively, representing increases of 39.9%, 36.4%, and 9.5% compared to that of EP/DA. These elevated E_a values underscored the pronounced inhibitory effects of Co^{2+}, Cu^{2+}, and Zn^{2+} on the curing reactivity of DA. Overall, the coordination between DA and transition metal ions reduces the curing reactivity of DA, with suppression varying based on the type of metal ion and coordination number.

The dynamic rheometer was employed to monitor how the viscosity of EP mixtures varied under heating, with results illustrated in Fig. 2f-i and summarized in Table S4. This measurement offered valuable information on the gelation behavior and thermal latency of EP/M-DA systems, key performance metrics for single-component epoxy resins. Gelation temperature (T_v) and gelation time, representing the onset of crosslinked network formation, serve as critical indicators of thermal latency in single-component epoxy resins. A higher T_v and extended gelation time signify improved thermal latency, enabling better control over storage stability and curing performance in practical applications [13, 30]. EP/Fe-DA exhibited a T_v of 126.1 °C, similar to that of EP/DA at 125.5 °C. However, T_v values for EP/Co-DA, EP/Ni-DA, EP/Cu-DA, and EP/Zn-DA were increased to 141.6, 189.5, 198.5, and 134.6 °C, respectively, indicating

enhanced thermal latency (see Fig. 2f and Table S4). Rheological testing at 50 °C, simulating challenging storage conditions, showed that EP/DA gelled within 203 minutes, whereas EP/Fe-DA, though not gelled, displayed a notable viscosity increase, indicating a slight improvement in thermal latency. By contrast, EP/Co-DA, EP/Ni-DA, EP/Cu-DA, and EP/Zn-DA showed no significant viscosity change at 50 °C, demonstrating improved thermal latency and processability at lower temperatures (see Fig. 2g). Conversely, EP/M-DA mixtures rapidly gelled within 30 minutes at 100 or 150 °C, demonstrating efficient curing at elevated temperatures (see Fig. 2h). To estimate the shelf life of the EP mixtures, viscosity changes at 25 °C were monitored over time, presented in Fig. 2i and Table S4. EP/DA displayed a short shelf life of 2 days. Upon the introduction of metal ions, the shelf life of EP/Fe-DA slightly increased to 3 days, while the shelf life of EP/Co-DA, EP/Ni-DA, EP/Cu-DA, and EP/Zn-DA was significantly extended to 31, 37, 43, and 12 days, respectively. These results highlight the crucial influence of metal-imidazole coordination in enhancing latency. The observed order of latency improvement among the EP/M-DA systems, EP/Cu-DA (43 days) > EP/Ni-DA (37 days) > EP/Co-DA (31 days) > EP/Zn-DA (12 days) > EP/Fe-DA (3 days), reflects the unique coordination structures and thermal stabilities of different M-DA complexes. These differences provide a valuable basis for designing advanced single-component epoxy systems with tailored latency profiles.

3.3. Thermal properties

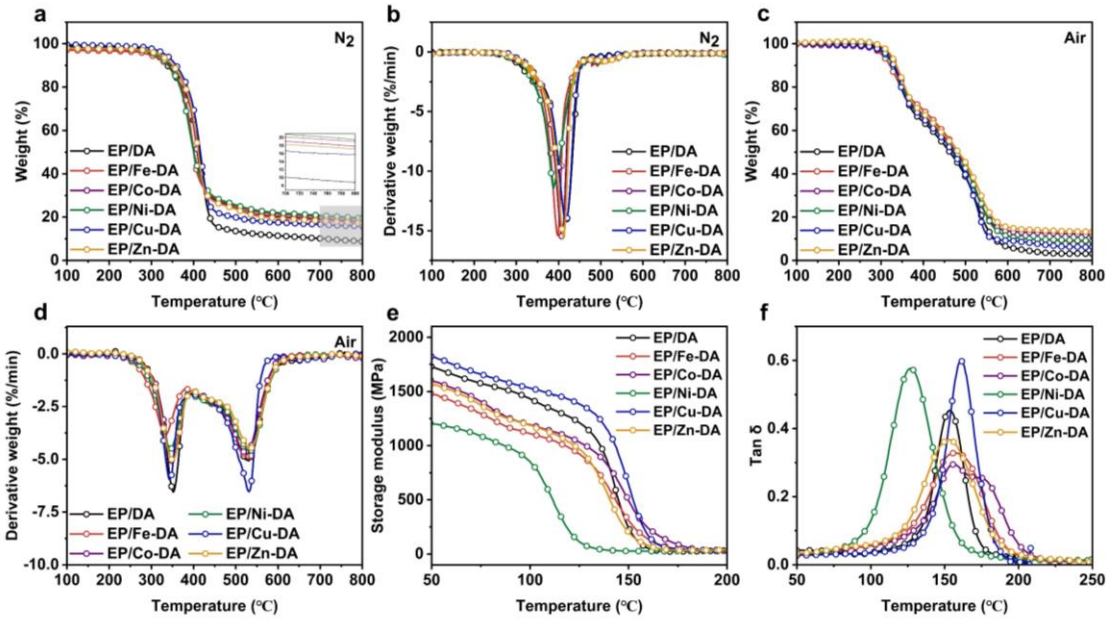

Fig. 3. (a, c) TGA and (b, d) DTG plots under nitrogen and air atmosphere; (e) storage modulus (*E'*) and (f) Tanδ curves of EP thermosets.

Thermal stability of the EP thermosets was evaluated through thermogravimetric analysis (TGA), and the corresponding results summarized in Fig. 3 and Table S5. Under nitrogen flow, EP/M-DA thermosets exhibited differences in thermal parameters, resulting from the incorporation of transition metal elements. Significant differences were noted in the temperature at 5% weight loss ($T_{5\%}$), as presented in Fig. 3a and detailed in Table S5. The $T_{5\%}$ of EP/Fe-DA decreased to 295.1 °C, showing a decrease of 16.3 °C compared to EP/DA. In contrast, $T_{5\%}$ values for other EP/M-DA were either retained or increased. Among all EP thermosets, EP/Cu-DA exhibited the highest $T_{5\%}$ at 333.4 °C, surpassing EP/DA by 22 °C, indicative of enhanced thermal stability. Additionally, the temperatures at the maximum weight loss rate (T_{max}s) of EP/M-DA thermosets slightly decreased, likely attributed to the phosphorus components' catalytic dehydration effect and the decomposition-facilitating role of transition metal ions. [19,

30, 44]. It is important to note that the combined influence of phosphorus and metal elements greatly improved the carbonization process in EP/M-DA thermosets, as evidenced by the higher char yield (see Fig. 3b). The char yield at 800 °C (*CY*) exhibited a notable increase in EP/M-DA, rising from 8.9 wt% in EP/DA to a range of 15.9-19.5 wt% (see Table S5). This improvement underscores the critical role of transition metal ions in promoting condensed-phase flame retardancy [45, 46]. Under an air atmosphere, EP/M-DA demonstrated slightly reduced $T_{5\%}$ values, lower maximum weight loss rates, and increased char yields (*CY*) relative to the reference sample (Fig. 3c and d). These findings suggest that, for the same phosphorus content, the addition of metal ions further enhances char formation, beneficial for improving condensed-phase flame retardancy.

Dynamic mechanical analysis (DMA) was used to measure the thermodynamic properties of EP thermosets, with the results shown in Fig. 3e and f and summarized in Table S6. Among all EP thermosets, EP/Cu-DA exhibited the highest *E'* at 50 °C (1823 MPa), outperforming other M-DA systems and suggesting the establishment of a highly robust and thermally stable crosslinking network. In contrast, the *E'* values for EP/Fe-DA, EP/Co-DA, and EP/Zn-DA decreased by 15.2%, 8.1%, and 10.1%, respectively, relative to EP/DA, while EP/Ni-DA showed a more pronounced reduction of 30.8% (see Fig. 3e). Furthermore, EP/Cu-DA achieved the highest glass transition temperature (T_g) among all EP thermosets at 160.9 °C, exceeding the T_g of EP/DA at 154.2 °C. EP/Fe-DA, EP/Co-DA, and EP/Zn-DA exhibited T_g values close to that of EP/DA, with values of 157.0, 156.3, and 152.7 °C, respectively. However, EP/Ni-DA showed a

significant decrease in T_g, dropping by 27.3 °C to 126.9 °C (see Fig. 3f). Overall, introducing transition metal elements greatly enhanced the char formation capability of all EP/M-DA thermosets in comparison to EP/DA. However, among these systems, only EP/Cu-DA achieved superior heat resistance and mechanical rigidity. Other EP/M-DA thermosets exhibited moderate or reduced thermal stability, reflecting the varying coordination behaviors and dissociation kinetics of different metal ions.

3.4. Mechanical properties

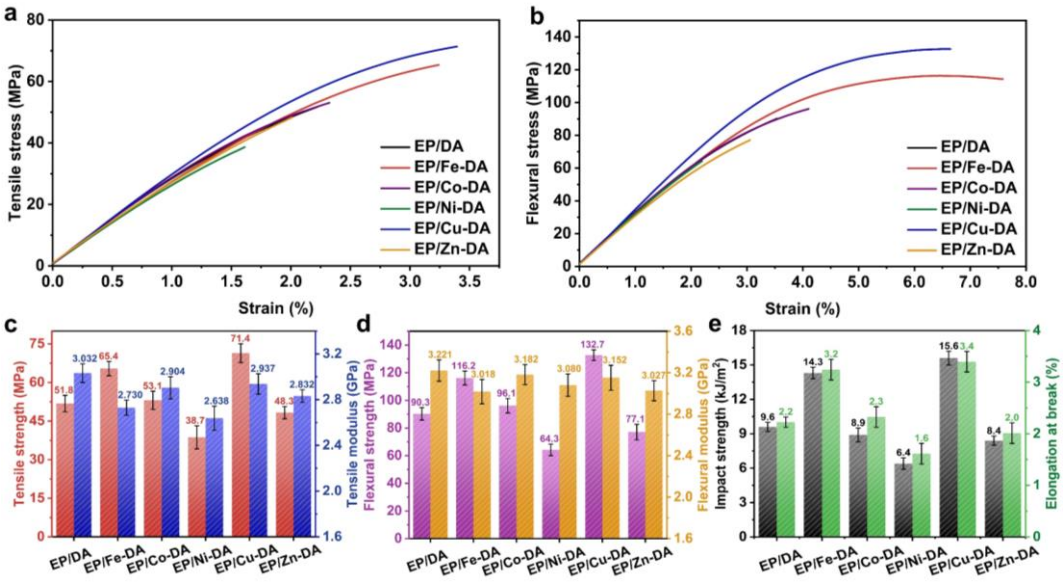

Fig. 4. Stress-strain curves for (a) tensile testing and (b) flexural testing; (c) tensile strength and modulus values; (d) flexural strength and modulus values; and (e) impact strength and elongation at break data for EP thermosets.

The mechanical properties of EP thermosets are summarized in Fig. 4 and Table S7. Among the EP/M-DA thermosets, EP/Fe-DA and EP/Cu-DA demonstrated significant improvements in tensile strength, reaching 65.4 MPa (26.3% increase) and 71.4 MPa (37.8% increase), respectively, compared to EP/DA (51.8 MPa). In contrast, EP/Co-DA exhibited a marginal improvement of 2.5%, while EP/Ni-DA and EP/Zn-

DA showed declines of 25.3% and 6.8%, respectively. All EP/M-DA thermosets showed some reduction in tensile modulus to varying degrees. Notably, EP/Ni-DA exhibited the most pronounced decline in tensile modulus, with a reduction of 13.0% compared to EP/DA, indicating a decrease in network rigidity and structural integrity. Similar trends emerged in the flexural properties of the EP/M-DA thermosets, with EP/Cu-DA consistently showing the highest flexural strength improvement. In Fig. 4b and d, the flexural strengths of EP/Fe-DA, EP/Co-DA, and EP/Cu-DA increased by 28.7%, 6.4%, and 47.0%, respectively, whereas EP/Ni-DA and EP/Zn-DA exhibited reductions of 28.8% and 14.6%. Additionally, EP/Fe-DA and EP/Cu-DA exhibited remarkable improvements in toughness, demonstrated by significant increases in elongation at break and impact strength. Specifically, the impact strengths of EP/Fe-DA and EP/Cu-DA increased to 14.3 kJ/m^2 and 15.6 kJ/m^2, respectively, marking a considerable leap from the 9.6 kJ/m^2 recorded for EP/DA (see Fig. 4e and Table S7). These enhancements are probably ascribed to the effective energy absorption mechanisms introduced by metal-ligand interactions in these thermosets [19, 30].

The variations in mechanical properties among EP/M-DA thermosets are probably influenced by two primary factors. First, during curing, transition metal ions interact with oxygen atoms in epoxy groups or alkoxide anions formed during imidazole-catalyzed polymerization, which can deactivate active centers and modulate the curing kinetics [47, 48]. This effect is particularly pronounced in EP/Ni-DA, resulting in reduced crosslinking density and diminished mechanical performance. Second, in the cured network, transition metal ions form coordination bonds with nitrogen atoms in

imidazole groups or oxygen atoms in the epoxy resin [19, 30]. These coordination bonds act as sacrificial energy-dissipating units under applied external forces, improving the strength and toughness of EP/Fe-DA and EP/Cu-DA. The effectiveness of this mechanism varies depending on the type of metal ion, with Cu^{2+} displaying the most effective energy absorption, consistent with its superior mechanical properties. The degree of these two effects varies with the type of metal ion, resulting in distinct mechanical characteristics in the cured products. Overall, the incorporation of transition metal ions generally reduces the stiffness of EP/M-DA thermosets, while EP/Fe-DA and EP/Cu-DA demonstrate significant improvements in strength and toughness, highlighting the dual role of metal ions in modulating curing kinetics and enhancing energy dissipation mechanisms. These findings provide insights for designing advanced epoxy thermosets with customized mechanical performance.

3.5. Flame retardancy and smoke suppression

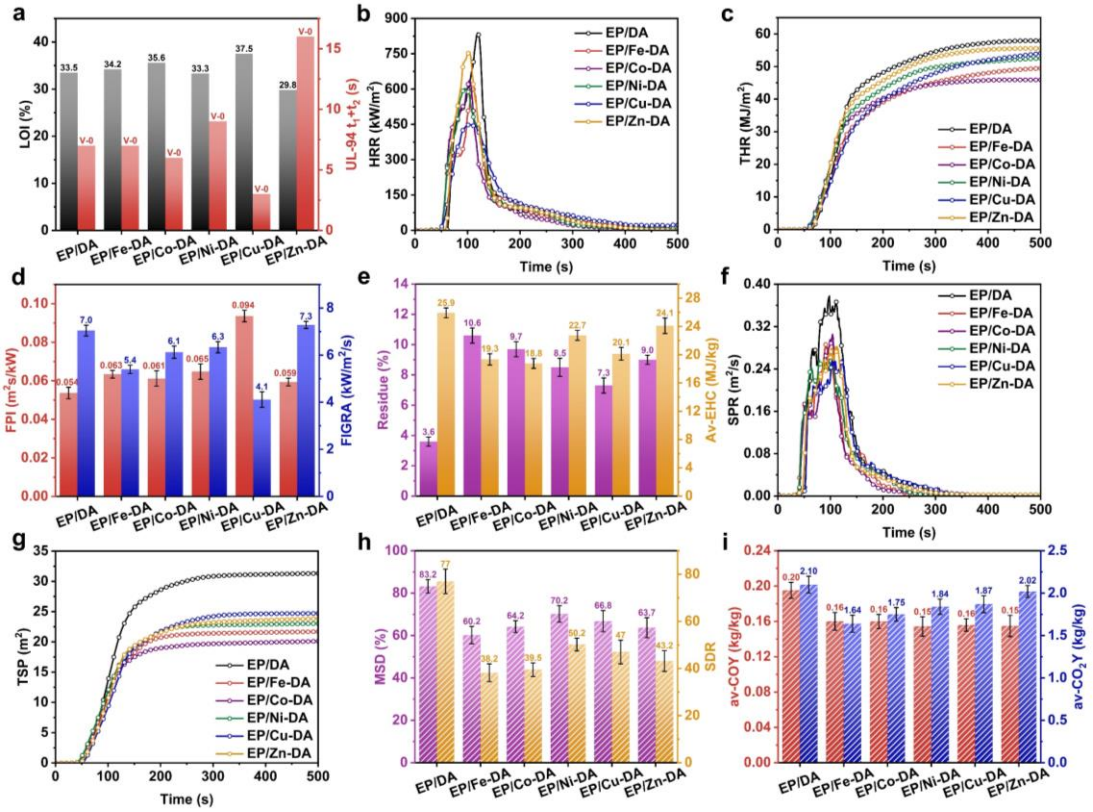

Fig. 5. (a) LOI values and UL-94 ratings; (b) heat release rate (HRR) curves; (c) total heat release (THR) curves; (d) fire performance index (FPI) and fire growth rate index (FIGRA); (e) residue and average effective heat of combustion (Av-EHC); (f) smoke production rate (SPR) curves; (g) total smoke production (TSP) curves; (h) maximum smoke density (MSD) and smoke density rating (SDR); and (i) average carbon monoxide yield (av-COY) and average carbon dioxide yield (av-CO_2Y) of EP thermosets.

Fig. 5a highlights the LOI values and UL-94 ratings of the EP thermosets. With an LOI of 33.5% and a UL-94 V-0 rating, the EP/DA thermoset exhibited outstanding flame resistance, largely owing to the presence of phosphorus-containing groups, which impart substantial inherent fire-retardant characteristics. This establishes a strong baseline for evaluating the combined impact of transition metal ions and phosphorus in

enhancing the performance of EP/M-DA systems. For EP/M-DA thermosets, all samples also reached a UL-94 V-0 rating, with LOI values exceeding 29%. Specifically, EP/Fe-DA, EP/Co-DA, and EP/Cu-DA exhibited increased LOI values of 34.2%, 35.6%, and 37.5%, respectively, in comparison to EP/DA, indicating improved fire safety resulting from the combined effect of phosphorus and metal ions.

Table 2. The combustion parameters of EP samples.

Sample	TTI [a] (s)	PHRR [a] (kW/m^2)	THR (MJ/m^2)	PSPR [a] (m^2/s)	TSP (m^2)
EP/DA	45±2	838±18	57.9±1.9	0.377±0.022	31.3±0.4
EP/Fe-DA	38±4	599±23	49.5±3.0	0.289±0.034	21.7±0.2
EP/Co-DA	39±2	637±25	45.9±2.7	0.305±0.018	20.1±0.2
EP/Ni-DA	39±5	602±31	52.5±3.5	0.255±0.030	23.0±0.3
EP/Cu-DA	42±3	448±22	54.1±3.7	0.256±0.019	24.7±0.3
EP/Zn-DA	45±6	757±17	55.5±3.3	0.282±0.029	23.8±0.2

[a] TTI: time to ignition; PHRR: peak heat release rate; and PSPR: peak smoke production rate.

Cone calorimetry was employed to examine the combustion characteristics, specifically heat and smoke release, with comprehensive results summarized in Table 2 and Fig. 5b-g. EP/DA showed high PHRR and THR values of 838 kW/m^2 and 57.9 MJ/m^2, respectively. In contrast, incorporating metal complexes significantly lowered both metrics. Remarkably, EP/Cu-DA, despite having comparable phosphorus content, demonstrated superb flame-retardant properties, achieving the lowest PHRR of 448 kW/m^2 and a THR of just 54.1 MJ/m^2, underscoring its superior performance in fire safety applications. In addition to PHRR and THR, FPI and FIGRA are key benchmarks for evaluating flammability [4]. Materials with elevated FPI and reduced FIGRA values demonstrate significantly improved fire resistance and lower combustion risk [19, 49,

50]. As illustrated in Fig. 5d, incorporating M-DA complexes significantly enhanced fire performance, evident from the increased FPI and reduced FIGRA compared to EP/DA. Among all samples, EP/Cu-DA stood out with the highest FPI and the lowest FIGRA, underscoring its superb fire safety.

Av-EHC, a measure of combustion intensity in the gaseous phase, is presented in Fig. 5e. EP/DA displayed a relatively low Av-EHC of 25.9 MJ/kg, resulting from the gaseous-phase flame-retardant effects of DA [19, 22]. This value further decreased by 6.9%-27.4% in EP/M-DA thermosets, mainly driven by the metal ions' catalytic promotion of carbonization during burning. [24, 25]. This process promotes char formation, creating a protective layer that prevents combustible pyrolysis products from entering the flame zone [19]. As a result, EP/M-DA thermosets showed higher residual char than EP/DA, suggesting that the introduction of transition metal elements in addition to phosphorus further promotes char formation during combustion, acting as a barrier that inhibits flame propagation and enhances overall flame retardancy.

Given the importance of smoke toxicity in fire hazards, the smoke suppression capabilities of all EP thermosets were assessed using cone calorimetry and smoke density tests. The results, detailed in Fig. 5f-h and Table 2, revealed that EP/M-DA thermosets significantly outperformed EP/DA, showing marked decreases in PSPR and TSP values, highlighting their superior smoke-suppression performance. For example, EP/Cu-DA achieved PSPR and TSP reductions of 32.1% and 21.1%, respectively, relative to EP/DA (see Fig. 5f and g). Additionally, the inclusion of M-DA complexes significantly reduced the MSD and SDR values. Relative to EP/DA, the MSD of EP/M-

DA thermosets dropped by 15.6%-27.6%, while their SDR decreased by 34.8%-50.4% (see Fig. 5h). Among the EP thermosets, EP/Fe-DA showed the lowest MSD at 60.2% and the lowest SDR at 38.2, indicating superb smoke suppression. In Fig. 5i, EP/M-DA thermosets exhibited lower av-COY at around 0.15 kg/kg compared to 0.20 kg/kg in EP/DA, suggesting reduced smoke toxicity. Additionally, the av-CO_2Y of EP/M-DA decreased by 3.8%-21.9% compared to EP/DA, indicating that combustion was effectively suppressed, resulting in fewer complete oxidation products. To conclude, EP/M-DA thermosets showcased enhanced fire safety, as reflected by significant decline in heat release, smoke generation, and harmful gas emissions (eg. carbon monoxide). These findings underscore the efficacy of metal-phosphorus synergism in promoting condensed-phase carbonization and gaseous-phase combustion inhibition, offering a pathway for the creation of advanced, fire-resistant epoxy systems.

3.6. Flame-retardant actions

3.6.1. Condensed phase analysis

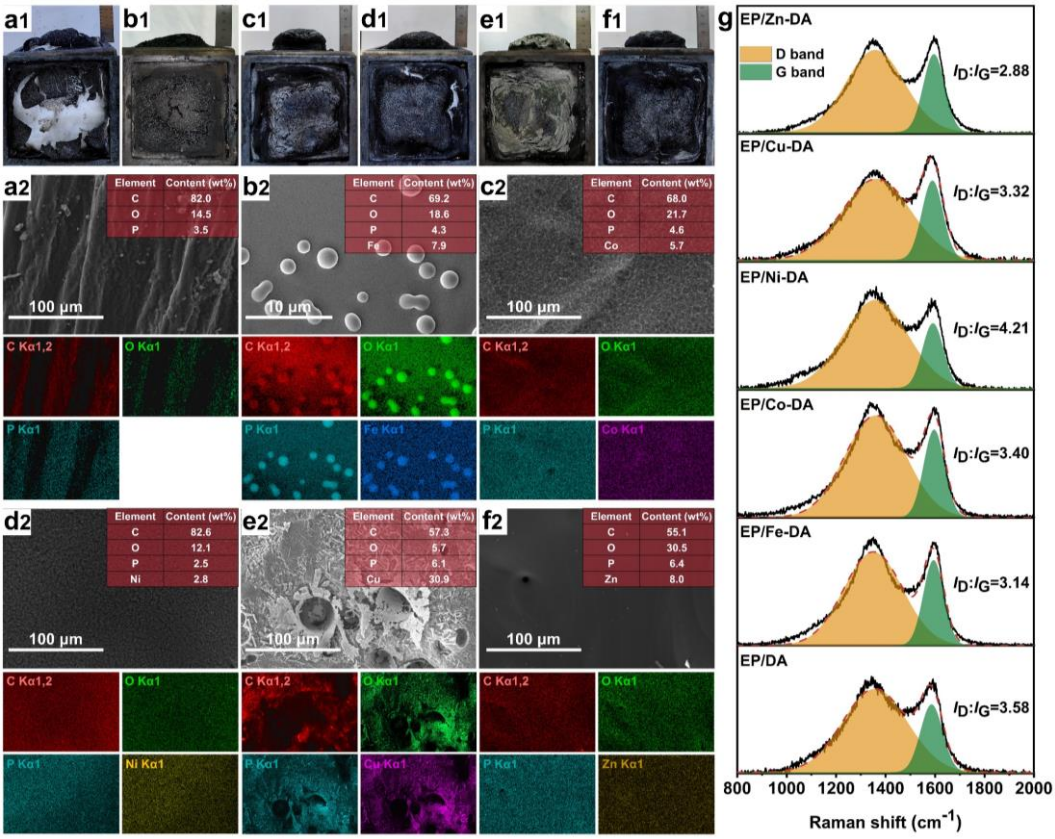

Fig. 6. Digital photographs and SEM images of char residues for (a_1, a_2) EP/DA, (b_1, b_2) EP/Fe-DA, (c_1, c_2) EP/Co-DA, (d_1, d_2) EP/Ni-DA, (e_1, e_2) EP/Cu-DA, and (f_1, f_2) EP/Zn-DA; and (g) Raman spectra of the residual chars.

To elucidate the role of M-DA complexes in the condensed phase, the residual chars obtained from cone calorimetry were comprehensively analyzed using digital imaging, scanning electron microscope (SEM), energy dispersive X-ray spectroscopy (EDS), X-ray diffraction (XRD), and X-ray photoelectron spectroscopy (XPS). Digital photographs of char residues are shown in Fig. 6a_1-f_1, with SEM images and elemental mappings of their external surfaces provided in Fig. 6a_2-f_2. EP/DA char displayed a compact but nearly consumed structure (see Fig. 6a_1 and a_2), indicating that the low-oxidation-state phosphorus groups in DA predominantly functioned in the gaseous phase, with limited involvement in promoting carbonization within the condensed

phase [15, 19, 22]. This limitation underscores the necessity of enhancing condensed-phase performance, achieved here by incorporating transition metal ions. The introduction of M-DA complexes markedly enhanced the charring ability of EP thermosets, compensating for the limited condensed-phase action of DA. This enhancement resulted in continuous and structurally stable char layers (see Fig. 6b_1-f_1). In Fig. 6b_2-f_2, the SEM images of EP/M-DA chars revealed compact and continuous external surfaces, which effectively shielded the underlying matrix from flame exposure. Furthermore, the elemental mappings of EP/M-DA chars confirmed the presence of phosphorus and transition metal elements, indicating their involvement in the carbonization process. Notably, EP/Fe-DA char exhibited spherical particles enriched with phosphorus, oxygen, and iron (see Fig. 6b_2), while dendritic crystals containing phosphorus, oxygen, and copper were observed in EP/Cu-DA char (see Fig. 6e_2). These high-surface-area inorganic metal particles improve the thermal stability of the char layer and may also serve as catalytic centers, facilitating various reactions during the combustion process [28, 29].

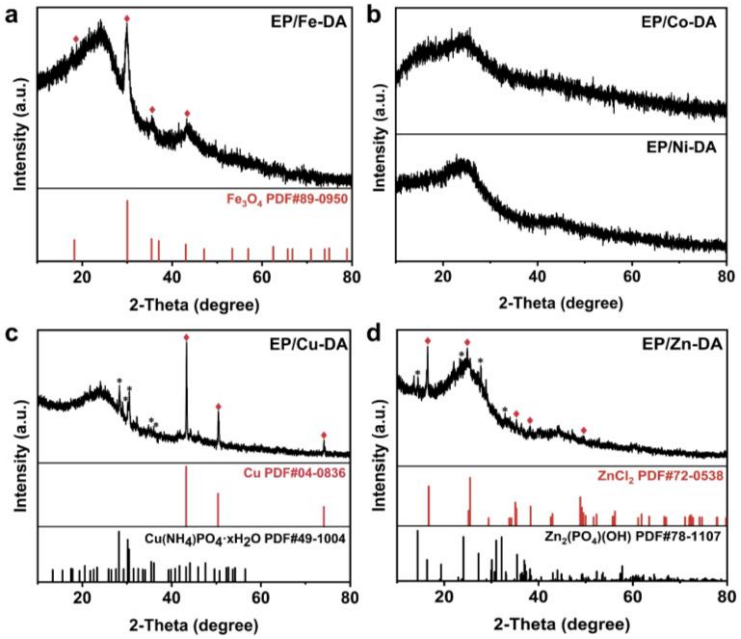

Fig. 7. XRD patterns of char residues after cone calorimetry for (a) EP/Fe-DA, (b) EP/Co-DA and EP/Ni-DA, (c) EP/Cu-DA, and (d) EP/Zn-DA.

In Fig. 6g, the Raman spectra of char residues revealed D and G peaks at 1356 and 1588 cm^{-1}, corresponding to disordered carbon and graphitic structures, respectively [2, 27]. The intensity ratio of the D peak to G peak (I_D/I_G) reflects the degree of graphitization [24]. Except for EP/Ni-DA, all EP/M-DA chars exhibited lower I_D/I_G ratios compared to EP/DA, indicating higher graphitization levels and improved thermal stability. Among the samples, EP/Zn-DA char achieved the smallest I_D/I_G values of 2.88, highlighting its superior carbonization performance. The XRD patterns of the residues from EP/M-DA thermosets are presented in Fig. 7. Fe_3O_4 was identified in EP/Fe-DA char (see Fig. 7a), while $Cu(NH_4)PO_4·xH_2O$ and metallic Cu were detected in EP/Cu-DA char (see Fig. 7c). The findings indicate that the redox cycles of metals (e.g., Cu^{2+}-Cu, Fe^{3+}-Fe^{2+}) occur during combustion. These cycles are likely associated with the interactions between metal compounds and reducing gases such as

CO and NO generated during pyrolysis [25, 28]. Additionally, the metals may act as catalysts, facilitating the oxidation and decomposition of organic components [24, 28]. This catalytic activity plays a significant role in mitigating smoke toxicity and reducing smoke production. In EP/Zn-DA char, $ZnCl_2$ and $Zn_2(PO_4)(OH)$ were detected (see Fig. 7d), which likely contributed to its enhanced thermal resistance. For EP/Co-DA and EP/Ni-DA chars, only a wide diffraction peak at 24°, associated with the (002) plane of graphite, was observed in their XRD patterns (see Fig. 7b).

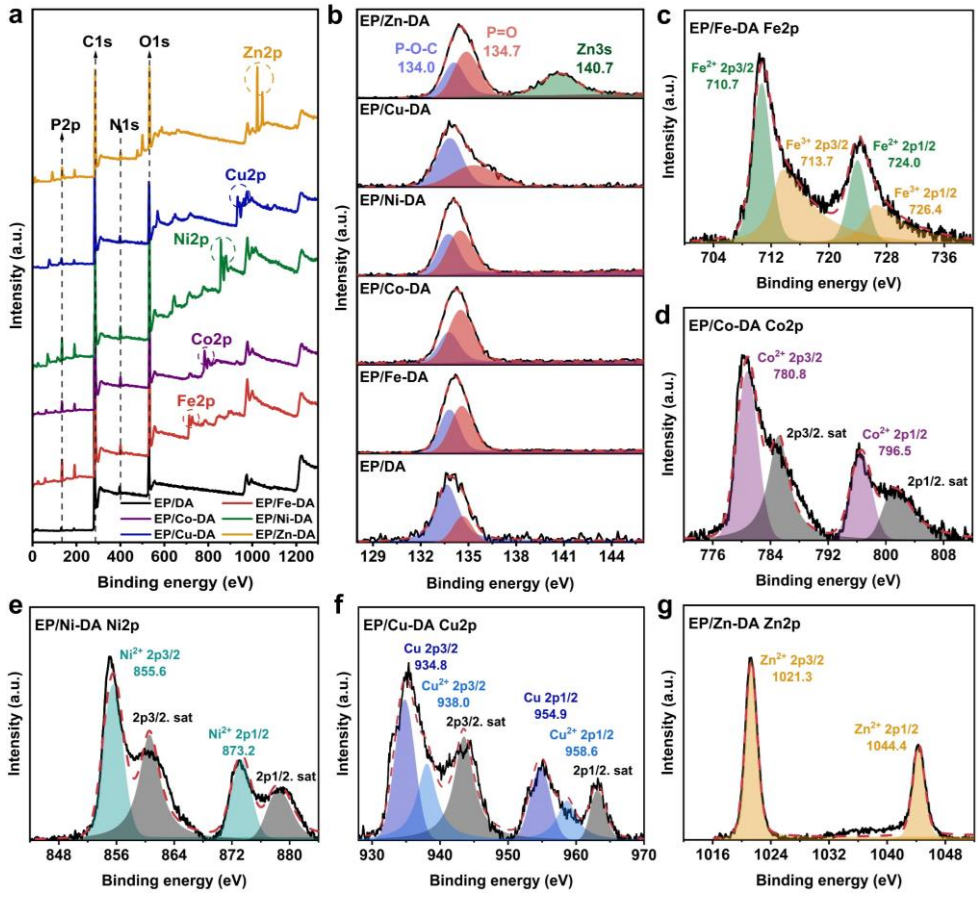

Fig. 8. (a) Full-scan XPS spectra and (b) high-resolution P2p XPS spectra of char residues; high-resolution XPS spectra of (c) Fe2p for EP/Fe-DA char, (d) Co2p for EP/Co-DA char, (e) Ni2p for EP/Ni-DA char, (f) Cu2p for EP/Cu-DA char, and (g) Zn2p for EP/Zn-DA char.

XPS analysis of the char residues provided additional insight with results shown in Fig. 8 and Fig. S8. All residual chars displayed similar chemical states of carbon, nitrogen, oxygen, and phosphorus, as evidenced by their C1s, N1s, O1s, and P2p spectra (see Fig. S3 and 8b). The C1s spectra exhibited peaks corresponded to C=C, C-H/C-C, C-N/C-O, and C=O bonds at 284.2, 284.8, 285.6, and 288.7 eV, respectively (see Fig. S3a) [14, 19]. The N1s spectra displayed peaks at 398.6 and 400.7 eV, attributed to C-N and N-H structures (see Fig. S3b), while the O1s spectra revealed peaks at 532.0 and 533.4 eV, associated with =O and -O- bonds (see Fig. S3c) [19, 30, 51]. The P2p spectra exhibited peaks at 134.0 and 134.7 eV, associated with P-O-C and P=O linkages, indicating phosphoric-oxygenic species were generated in combustion process (see Fig. 8b) [19, 20, 27]. In Fig. 8a and Table S8, the detection of transition metal elements in EP/M-DA residues further confirmed their involvement in the carbonization process, consistent with EDS results. The detailed analysis of the chemical states of transition metal elements in EP/M-DA char residues is presented in Fig. 8c-g. In Fig. 8c, peaks at 710.7 eV (2p3/2) and 713.7 eV (2p3/2) corresponded to Fe^{2+} and Fe^{3+}, respectively. In Fig. 8d, the presence of peaks at 780.8 eV (2p3/2), 785.1 eV (satellite peak of 2p3/2) [52], 796.5 eV (2p1/2), and 801.1 eV (satellite peak of 2p1/2) suggested the existence of Co^{2+} in the EP/Co-DA char [30]. Fig. 8e revealed peaks at 855.6 eV (2p3/2), 860.6 eV (satellite peak of 2p3/2), 873.2 eV (2p1/2), and 878.5 eV (satellite peak of 2p1/2), corresponding to Ni^{2+} in EP/Ni-DA char [24]. In Fig. 8f, the Cu2p spectra of EP/Cu-DA char confirmed the existence of Cu^{2+} and metallic Cu, as evidenced by the characteristic peaks at 934.8 eV (2p3/2) and 938.0 eV (2p3/2) [19, 33]. For EP/Zn-DA

char, Zn2p spectra revealed peaks at 1021.3 eV (2p3/2) and 1044.4 eV (2p1/2), confirming the existence of Zn^{2+} [30, 35]. These findings confirm that metal-derived species generated during the thermal decomposition of EP/M-DA thermosets significantly enhanced the flame resistance within the condensed phase. By catalyzing char formation and promoting graphitization, these metal-phosphorus synergistic systems produced continuous, thermally stable char layers that suppressed heat transfer, minimized smoke emissions, and inhibited flame spread, thus improving overall fire safety.

3.6.2. Gaseous phase analysis

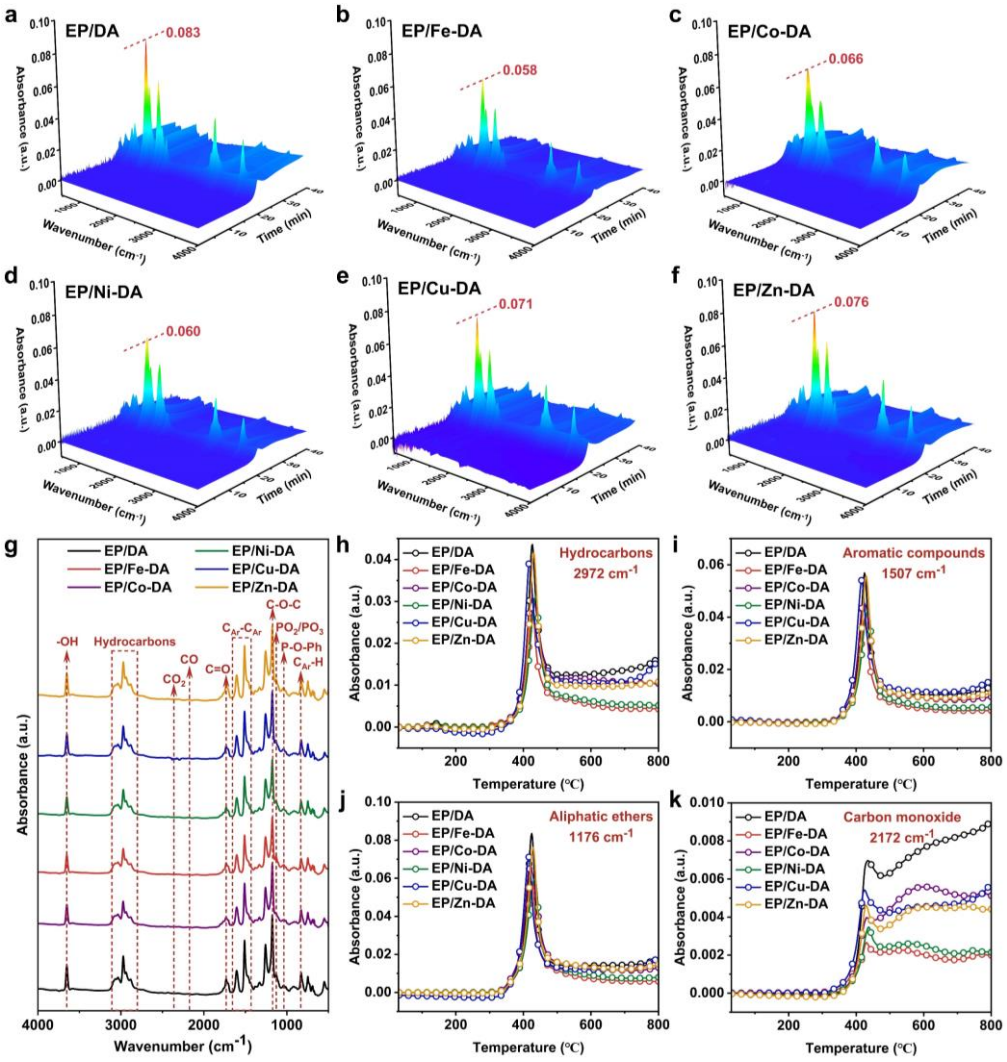

Fig. 9. 3D TG-FTIR spectra of (a) EP/DA, (b) EP/Fe-DA, (c) EP/Co-DA, (d) EP/Ni-DA, (e) EP/Cu-DA, and (f) EP/Zn-DA; (g) FTIR spectra at T_{max}; and absorbance-temperature plots at characteristic wavenumbers (h) 2972 cm^{-1}, (i) 1507 cm^{-1}, (j) 1176 cm^{-1}, and (k) 2172 cm^{-1}.

TG-FTIR analyses were performed to explore the flame-retardant behavior of M-DA complexes in the gaseous phase, with the detailed results provided in Fig. 9. As presented in Fig. 9g, the major volatiles emitted during the thermal degradation of all EP thermosets included water/phenol (3649 cm^{-1}), hydrocarbons (3109-2807 cm^{-1}), carbon dioxide (2362 cm^{-1}), carbon monoxide (2172 cm^{-1}), carbonyl compounds (1734 cm^{-1}), aromatic species (1598, 1511, and 828 cm^{-1}), and esters (1170 cm^{-1}) [19, 44, 51]. Additionally, all EP thermosets exhibited absorption peaks at 1130 cm^{-1} and 1034 cm^{-1}, corresponding to P=O and P-O-Ph bonds, respectively, demonstrating the release of phosphorus-containing fragments [14, 19, 20]. The detection of these volatiles confirms that the thermal cracking mechanisms of EP/DA and EP/M-DA were largely consistent, yet EP/M-DA thermosets exhibited notably lower volatile emissions (see Fig. 9a-f).

Compared to EP/DA, the reduced absorption intensities of hydrocarbons, aromatic compounds, and aliphatic ethers in the EP/M-DA spectra indicate that these volatile species were redirected towards catalytic carbonization instead of contributing to combustion in the gaseous phase (see Fig. 9h-j). This redirection was facilitated by the catalytic effects of transition metal ions, which enhanced carbonization and minimized the release of combustible volatiles, thereby improving fire resistance and reducing smoke production [19, 30, 51]. Furthermore, EP/M-DA thermosets demonstrated

decreased absorption intensity for carbon monoxide (2172 cm^{-1}) at 400-800 °C, suggesting reduced smoke toxicity (see Fig. 9k). This reduction can be attributed to two key factors: first, the generation of dense residual char inhibited combustion; second, the catalytic oxidation functions of transition metal elements at elevated temperatures facilitated the conversion of pyrolysis products into carbon dioxide, promoting more complete combustion. In the high-temperature region, transition metal compounds likely catalyzed soot oxidation, reducing smoke particle formation [19, 24, 28].

To the smoke-suppressing inhibition behavior of M-DA complexes, pyrolysis-gas chromatography/mass spectrometry (Py-GC/MS) analysis was performed on EP thermosets, with total ion chromatograms presented in Fig. S4. The main decomposition products, identified through retention times, are listed in Table S9-S14. Common pyrolysis products included short-chain hydrocarbons, aromatic compounds, and bisphenol A and its derivatives, which are typical fuel precursors in combustion. Furthermore, phosphorus-based compounds were found in all EP thermosets, emphasizing the quenching function of phosphorus radicals in inhibiting combustion in the gaseous phase. Interestingly, the pyrolysis of EP/M-DA thermosets indicated the presence of fused heterocyclic compounds and long-chain hydrocarbons after a retention time of 20 minutes, which were absent in the EP/DA thermoset. This suggests that the inclusion of metal compounds altered the pyrolysis pathways of the epoxy resin, potentially via catalytic mechanisms. Metal compounds, acting as Lewis acids, catalyzed radical reactions, rearrangements, and polymerization, leading to the formation of high-molecular-weight products [19, 25, 30]. This catalytic action reduced

the formation of smaller volatile species and redirecting pyrolysis intermediates towards condensed-phase reactions. The newly formed long-chain hydrocarbons and fused heterocyclic compounds exhibited lower volatility and higher thermal stability compared to smaller molecules. Consequently, their reduced volatility limited the release of flammable species into the gaseous phase, further contributing to decreased smoke release and enhanced flame-retardant performance.

4. Conclusion

This study systematically investigated the use of five metal-based phosphorus/imidazole-containing complexes (M-DA) as latent curing agents for the development of fire-safe single-component epoxy resin (EP) systems. By coordinating various transition metal ions (Fe^{3+}, Co^{2+}, Ni^{2+}, Cu^{2+}, and Zn^{2+}) into a phosphorus-containing imidazole (DA), the M-DA complexes were designed to enhance flame retardancy, smoke suppression, and latency, addressing critical challenges in single-component EP. The results demonstrated that the M-DA complexes significantly improved the latency of EP systems. All EP/M-DA mixtures exhibited prolonged shelf lives, with EP/Cu-DA achieving the longest storage duration of 43 days compared to 2 days for EP/DA. The trend in latency performance followed the order $Cu^{2+} > Ni^{2+} > Co^{2+} > Zn^{2+} > Fe^{3+}$, reflecting the influence of various metal ions on the curing kinetics. Quick gelation at elevated temperatures highlighted the suitability of M-DA complexes as effective latent curing agents.

For flame retardancy, all EP/M-DA thermosets revealed UL-94 V-0 ratings and high limiting oxygen index (LOI) values. Among them, EP/Cu-DA showed the most

significant improvements, with an LOI of 37.5%, a 46.5% reduction in peak heat release rate, and a 6.6% decrease in total heat release. Enhanced smoke suppression was observed across all EP/M-DA systems, with EP/Cu-DA reducing total smoke production by 21.1% and smoke density rating by 39.0%. These improvements were associated with the synergistic effects between transition metal ions and phosphorus, which promoted condensed-phase carbonization and gaseous-phase oxidation of pyrolysis products.

The study also revealed notable enhancements in mechanical properties for certain systems. EP/Cu-DA exhibited superior tensile and flexural strengths, increased elongation at break, and improved impact toughness, attributed to the optimized crosslinking density and metal-ligand interactions. However, variations in mechanical performance were observed depending on the type of metal ion, reflecting differences in their structural roles within the resin matrix.

In conclusion, the introduction of M-DA complexes provides a robust and versatile approach for improving the fire safety, storage stability, and mechanical properties of single-component EP systems. Among the tested systems, EP/Cu-DA exhibited the most balanced and exceptional performance, offering an innovative approach for developing advanced, high-performance single-component epoxy resins suitable for industrial applications requiring stringent fire safety standards.

Acknowledgements

We sincerely acknowledge the financial support from the National Natural Science Foundation of China (52473077), the Major Program of Hubei Province

(2023BAA028), the Australian Research Council (DE230100616 and DP240102628), and the Nonmetallic Excellence and Innovation Center (24PHD-4). We also extend our gratitude to Shiyanjia Lab (www.shiyanjia.com) for their essential assistance with the ICP-OES analyses.

References

[1] M. Gao, W. Wu, Y. Yan, Thermal degradation and flame retardancy of epoxy resins containing intumescent flame retardant, J. Therm. Anal. Calorim. 95(2) (2009) 605-608. https://doi.org/10.1007/s10973-008-9766-8.

[2] B. Yu, W.Y. Xing, W.W. Guo, S.L. Qiu, X. Wang, S.M. Lo, Y. Hu, Thermal exfoliation of hexagonal boron nitride for effective enhancements on thermal stability, flame retardancy and smoke suppression of epoxy resin nanocomposites via sol–gel process, J. Mater. Chem. A 4(19) (2016) 7330-7340. https://doi.org/10.1039/c6ta01565d.

[3] W.J. Yang, Q.J. Wu, Y. Zhou, S.E. Zhu, C.X. Wei, H.D. Lu, W. Yang, R.K.K. Yuen, Multifunctional phosphorus-containing porphyrin dye for efficiently improving the thermal, toughness, flame retardant and dielectric properties of epoxy resins, Prog. Org. Coat. 186 (2024) 107967. https://doi.org/10.1016/j.porgcoat.2023.107967.

[4] G.F. Ye, S.Q. Huo, C. Wang, Q. Zhang, B.T. Wang, Z.H. Guo, H. Wang, Z.T. Liu, Fabrication of flame-retardant, strong, and tough epoxy resins by solvent-free polymerization with bioderived, reactive flame retardant, Sustainable Mater. Technol. 39 (2024) e00853. https://doi.org/10.1016/j.susmat.2024.e00853.

[5] S. Qiu, X. Wang, B. Yu, X.M. Feng, X.W. Mu, R.K.K. Yuen, Y. Hu, Flame-retardant

-wrappedpolyphosphazene nanotubes: A novel strategy for enhancing the flame retardancy and smoke toxicity suppression of epoxy resins, J. Hazard. Mater. 325 (2017) 327-339. https://doi.org/10.1016/j.jhazmat.2016.11.057.

[6] S. Levchik, A. Piotrowski, E. Weil, Q. Yao, New developments in flame retardancy of epoxy resins, Polym. Degrad. Stab. 88(1) (2005) 57-62. https://doi.org/10.1016/j.polymdegradstab.2004.02.019.

[7] J.S. Wang, S.Q. Huo, J. Wang, S. Yang, K.W. Chen, C. Li, D. Fang, Z.P. Fang, P.G. Song, H. Wang, Green and Facile Synthesis of Bio-Based, Flame-Retardant, Latent Imidazole Curing Agent for Single-Component Epoxy Resin, ACS Appl. Polym. Mater. 4(5) (2022) 3564-3574. https://doi.org/10.1021/acsapm.2c00138.

[8] Y. Xu, W.J. Yang, Q.K. Zhou, T.Y. Gao, G.M. Xu, Q.L. Tai, S.E. Zhu, H.D. Lu, R.K.K. Yuen, W. Yang, C.X. Wei, Highly thermo-stable resveratrol-based flame retardant for enhancing mechanical and fire safety properties of epoxy resins, Chem. Eng. J. 450 (2022) 138475. https://doi.org/10.1016/j.cej.2022.138475.

[9] K. Kudo, S. Fuse, M. Furutani, K. Arimitsu, Imidazole-Type Thermal Latent Curing Agents with High Miscibility for One-Component Epoxy Thermosetting Resins, J. Polym. Sci., Part A: Polym. Chem. 54(17) (2016) 2680-2688. https://doi.org/10.1002/pola.28146.

[10] L.A. White, J.W. Weber, L.J. Mathias, Synthesis and thermal characterization of a one component maleimide-epoxy resin, Polym. Bull. 46(6) (2001) 463-469. https://doi.org/10.1007/s002890170033.

[11] Y.R. Wang, W.S. Liu, Y.P. Qiu, Y. Wei, A One-Component, Fast-Cure, and

Economical Epoxy Resin System Suitable for Liquid Molding of Automotive Composite Parts, Materials 11(5) (2018) 685. https://doi.org/10.3390/ma11050685.

[12] J.S. Wang, X. Chen, J. Wang, S. Yang, K.W. Chen, L. Zhu, S.Q. Huo, P.A. Song, H. Wang, High-performance, intrinsically fire-safe, single-component epoxy resins and carbon fiber reinforced epoxy composites based on two phosphorus-derived imidazoliums, Polym. Degrad. Stab. 208 (2023) 110261. https://doi.org/10.1016/j.polymdegradstab.2023.110261.

[13] Y. Xu, J. Wang, Y. Tan, M. Qi, L. Chen, Y. Wang, A novel and feasible approach for one-pack flame-retardant epoxy resin with long pot life and fast curing, Chem. Eng. J. 337 (2018) 30-39. https://doi.org/10.1016/j.cej.2017.12.086.

[14] Y. Xu, X. Shi, J. Lu, M. Qi, D. Guo, L. Chen, Y. Wang, Novel phosphorus-containing imidazolium as hardener for epoxy resin aiming at controllable latent curing behavior and flame retardancy, Compos. Pt. B-Eng. 184 (2020) 107673. https://doi.org/10.1016/j.compositesb.2019.107673.

[15] S. Huo, P. Song, B. Yu, S. Ran, V.S. Chevali, L. Liu, Z. Fang, H. Wang, Phosphorus-containing flame retardant epoxy thermosets: recent advances and future perspectives, Prog. Polym. Sci. 114 (2021) 101366. https://doi.org/10.1016/j.progpolymsci.2021.101366.

[16] J. Sag, D. Goedderz, P. Kukla, L. Greiner, F. Schoenberger, M. Doering, Phosphorus-Containing Flame Retardants from Biobased Chemicals and Their Application in Polyesters and Epoxy Resins, Molecules 24(20) (2019) 3746. https://doi.org/10.3390/molecules24203746.

[17] L. Chen, C. Ruan, R. Yang, Y.-Z. Wang, Phosphorus-containing thermotropic liquid crystalline polymers: a class of efficient polymeric flame retardants, Polym. Chem. 5(12) (2014) 3737-3749. https://doi.org/10.1039/c3py01717f.

[18] T. Sai, X. Ye, B. Wang, Z. Guo, J. Li, Z. Fang, S. Huo, Transparent, intrinsically fire-safe yet impact-resistant poly(carbonates-b-siloxanes) containing Schiff-base and naphthalene-sulfonate, J. Mater. Sci. Technol. 225 (2024) 11-20. https://doi.org/10.1016/j.jmst.2024.11.023.

[19] J.S. Wang, J. Wang, S. Yang, C.Q. Wu, X. Chen, K.W. Chen, P.A. Song, H. Wang, S.Q. Huo, Development of single-component epoxy resin with superb thermal stability, flame retardancy, smoke suppression, and latency via Cu-based phosphorus/imidazole-containing complex, Polym. Degrad. Stab. 228 (2024) 110906. https://doi.org/10.1016/j.polymdegradstab.2024.110906.

[20] J.S. Wang, J. Wang, F.Y. Wang, S. Yang, C.Q. Wu, X. Chen, K.W. Chen, P.A. Song, H. Wang, S.Q. Huo, Liquid phosphorus-based bis-imidazole compounds as latent curing agents for enhancing thermal, mechanical, and flame-retardant performances of single-component epoxy resins, Polym. Degrad. Stab. 230 (2024) 111066. https://doi.org/10.1016/j.polymdegradstab.2024.111066.

[21] J.S. Wang, J. Wang, S. Yang, K.W. Chen, Single-component flame-retardant and smoke-suppressive epoxy resins enabled by an aluminum/phosphorus/imidazole-containing complex, Compos. Pt. B-Eng. 253 (2023) 110571. https://doi.org/10.1016/j.compositesb.2023.110571.

[22] S. Huo, S. Yang, J. Wang, J. Cheng, Q. Zhang, Y. Hu, G. Ding, Q. Zhang, P. Song,

A liquid phosphorus-containing imidazole derivative as flame-retardant curing agent for epoxy resin with enhanced thermal latency, mechanical, and flame-retardant performances, J. Hazard. Mater. 386 (2020) 121984. https://doi.org/10.1016/j.jhazmat.2019.121984.

[23] Z. Xu, L. Duan, Y. Hou, F. Chu, S. Jiang, W. Hu, L. Song, The influence of carbon-encapsulated transition metal oxide microparticles on reducing toxic gases release and smoke suppression of rigid polyurethane foam composites, Composites Part A 131 (2020) 105815. https://doi.org/10.1016/j.compositesa.2020.105815.

[24] L. Zhang, S. Chen, Y.-T. Pan, S. Zhang, S. Nie, P. Wei, X. Zhang, R. Wang, D.-Y. Wang, Nickel Metal-Organic Framework Derived Hierarchically Mesoporous Nickel Phosphate toward Smoke Suppression and Mechanical Enhancement of Intumescent Flame Retardant Wood Fiber/Poly(lactic acid) Composites, ACS Sustainable Chem. Eng. 7(10) (2019) 9272-9280. https://doi.org/10.1021/acssuschemeng.9b00174.

[25] L. Wang, L. Song, Y. Hu, R.K.K. Yuen, Influence of Different Metal Oxides on the Thermal, Combustion Properties and Smoke Suppression in Ethylene-Vinyl Acetate, Ind. Eng. Chem. Res. 52(23) (2013) 8062-8069. https://doi.org/10.1021/ie400586t.

[26] G. Zhang, W. Wu, M. Yao, Z. Wu, Y. Jiao, H. Qu, Novel triazine-based metal-organic frameworks: Synthesis and mulifunctional application of flame retardant, smoke suppression and toxic attenuation on EP, Materials & Design 226 (2023) 111664. https://doi.org/10.1016/j.matdes.2023.111664.

[27] F. Xiao, K. Wu, F. Luo, S. Yao, M. Lv, H. Zou, M. Lu, Influence of Ionic Liquid-Based Metal-Organic Hybrid on Thermal Degradation, Flame Retardancy, and Smoke

Suppression Properties of Epoxy Resin Composites, J. Mater. Sci. 53(14) (2018) 10135-10146. https://doi.org/10.1007/s10853-018-2318-0.

[28] Z. Chen, T. Chen, Y. Yu, Q. Zhang, Z. Chen, J. Jiang, Metal-organic framework MIL-53 (Fe)@C/graphite carbon nitride hybrids with enhanced thermal stability, flame retardancy, and smoke suppression for unsaturated polyester resin, Polym. Adv. Technol. 30(9) (2019) 2458-2467. https://doi.org/10.1002/pat.4693.

[29] B. Li, A study of the thermal decomposition and smoke suppression of poly(vinyl chloride) treated with metal oxides using a cone calorimeter at a high incident heat flux, Polym. Degrad. Stab. 78(2) (2002) 349-356. https://doi.org/10.1016/s0141-3910(02)00185-4.

[30] J.-H. Lu, Y.-J. Xu, L. Chen, J.-H. Chen, J.-H. He, Z. Li, S.-L. Li, Y.-Z. Wang, Facile fabrication of intrinsically fire-safety epoxy resin cured with phosphorus-containing transition metal complexes for flame retardation, smoke suppression, and latent curing behavior, Chem. Eng. J. 442 (2022) 136097. https://doi.org/10.1016/j.cej.2022.136097.

[31] I. Hamerton, B.J. Howlin, J.R. Jones, S. Liu, J.M. Barton, Effect of complexation with copper (II) on cured neat resin properties of a commercial epoxy resin using modified imidazole curing agents, J. Mater. Chem. 6(3) (1996) 305-310. https://doi.org/10.1039/JM9960600305.

[32] M.L. Kaplan, A.L. Wayda, A.M. Lyons, Lanthanide–imidazole complexes as latent curing agents for epoxy resins, Polymer Science Part A: Polymer Chemistry 28(4) (1990) 731-40. https://doi.org/10.1002/pola.1990.080280404.

[33] B. Yang, Y.Y. Mao, Y.H. Zhang, G.F. Bian, L.Y. Zhang, Y. Wei, Q.R. Jiang, Y.P.

Qiu, W.S. Liu, A novel liquid imidazole-copper (II) complex as a thermal latent curing agent for epoxy resins, Polymer 178 (2019) 121586. https://doi.org/10.1016/j.polymer.2019.121586.

[34] J. Brown, I. Hamerton, B.J. Howlin, Preparation, characterization, and thermal properties of controllable metal-imidazole complex curing agents for epoxy resins, J. Appl. Polym. Sci. 75(2) (2000) 201-217. https://doi.org/10.1002/(sici)1097-4628(20000110)75:2.

[35] R.K. Jian, F.Q. Pang, Y.C. Lin, W.B. Bai, Facile construction of lamellar-like phosphorus-based triazole-zinc complex for high-performance epoxy resins, J. Colloid Interface Sci. 609 (2022) 513-522. https://doi.org/10.1016/j.jcis.2021.11.054.

[36] R. Yan, X. Gao, W. He, R. Guo, R.N. Wu, Z.Z. Zhao, H.Y. Ma, A simple and convenient method to fabricate new types of phytic acid-metal conversion coatings with excellent anti-corrosion performance on the iron substrate, Rsc Advances 7(65) (2017) 41152-41162. https://doi.org/10.1039/c7ra06186b.

[37] S.H. Sumrra, A. Suleman, Z.H. Chohan, M.N. Zafar, M.A. Raza, T. Iqbal, Triazole Metal Based Complexes as Antibacterial/Antifungal Agents, Russ. J. Gen. Chem. 87(6) (2017) 1281-1287. https://doi.org/10.1134/s107036321706024x.

[38] G.A. Sundaram, S. Kumaravelu, W.L. Tseng, P.V. Pham, A.S.K. Kumar, V. Parimelazhagan, Fine-Tuned Graphene Oxide Nanocomposite: Harnessing Copper(II)-Imidazole Complex for Enhanced Biological Responses and Balanced Photocatalytic Functionality, Materials 17(4) (2024) 892. https://doi.org/10.3390/ma17040892.

[39] T.D. George, W.W. Wendlandt, The thermal decomposition of metal complexes—

II Some ammine and ethylenediamine complexes of nickel (II), J. Inorg. Nucl. Chem. 25(4) (1963) 395-405. https://doi.org/10.1016/0022-1902(63)80190-6.

[40] W.W. Wendlandt, C.Y. Chou, The thermal decomposition of metal complexes—XI: The hexamminechromium (III) complexes, J. Inorg. Nucl. Chem. 26(6) (1964) 943-949. https://doi.org/10.1016/0022-1902(64)80255-4.

[41] S.Y. Du, Z.S. Guo, B.M. Zhang, Z.J. Wu, Cure kinetics of epoxy resin used for advanced composites, Polym. Int. 53(9) (2004) 1343-1347. https://doi.org/10.1002/pi.1533.

[42] K. Leena, P.B. Soumyamol, M. Baby, S. Suraj, R. Rajeev, D.S. Mohan, Non-isothermal cure and decomposition kinetics of epoxy-imidazole systems, J. Therm. Anal. Calorim. 130(2) (2017) 1053-1061. https://doi.org/10.1007/s10973-017-6410-5.

[43] W.W. Wendlandt, T.D. George, K.V. Krishnamurty, The thermal decomposition of metal complexes—I: Thermogravimetric and differential thermal analysis studies, J. Inorg. Nucl. Chem. 21(1) (1961) 69-76. https://doi.org/10.1016/0022-1902(61)80415-6.

[44] C. Wang, S.Q. Huo, G.F. Ye, B.T. Wang, Z.H. Guo, Q. Zhang, P.A. Song, H. Wang, Z.T. Liu, Construction of an epoxidized, phosphorus-based poly(styrene butadiene styrene) and its application in high-performance epoxy resin, Compos. Pt. B-Eng. 268 (2024) 111075. https://doi.org/10.1016/j.compositesb.2023.111075.

[45] X.H. Gan, J. Wang, S. Yang, X. Chen, J.S. Wang, K.W. Chen, Y.G. Zhang, L. Zhu, L. Xu, S.Q. Huo, Breaking the trade-off between mechanical properties and fire safety of epoxy resins based on phosphaphenanthrene derivatives by covalent crosslinking,

Polym. Degrad. Stab. 220 (2024) 110634. https://doi.org/10.1016/j.polymdegradstab.2023.110634.

[46] X. Bi, H. Di, J. Liu, Y.F. Meng, Y.Y. Song, W.H. Meng, H.Q. Qu, L.D. Fang, P.A. Song, J.Z. Xu, A core-shell-structured APP@COFs hybrid for enhanced flame retardancy and mechanical property of epoxy resin (EP), Adv. Compos. Hybrid Mater. 5(3) (2022) 1743-1755. https://doi.org/10.1007/s42114-021-00411-0.

[47] T. Vidil, F. Tournilhac, S. Musso, A. Robisson, L. Leibler, Control of reactions and network structures of epoxy thermosets, Prog. Polym. Sci. 62 (2016) 126-179. https://doi.org/10.1016/j.progpolymsci.2016.06.003.

[48] M. Döring, U. Arnold, Polymerization of epoxy resins initiated by metal complexes, Polym. Int. 58(9) (2009) 976-988. https://doi.org/10.1002/pi.2618.

[49] J.S. Wang, J. Wang, S. Yang, X. Chen, K.W. Chen, G. Zhou, X. Liu, L. Xu, S.Q. Huo, P.G. Song, H. Wang, Multifunctional phosphorus-containing imidazoliums endowing one-component epoxy resins with superior thermal latency, heat resistance, mechanical properties, and fire safety, Chem. Eng. J. 485 (2024) 149852. https://doi.org/10.1016/j.cej.2024.149852.

[50] C. Wang, S.Q. Huo, G.F. Ye, Q. Zhang, C.F. Cao, M. Lynch, H. Wang, P.A. Song, Z.T. Liu, Strong self-healing close-loop recyclable vitrimers via complementary dynamic covalent/non-covalent bonding, Chem. Eng. J. 500 (2024) 157418. https://doi.org/10.1016/j.cej.2024.157418.

[51] T. Sai, Y.K. Su, H.F. Shen, S.Y. Ran, S.Q. Huo, Z.H. Guo, Z.P. Fang, Fabrication and Mechanism Study of Cerium-Based P, N-Containing Complexes for Reducing Fire

Hazards of Polycarbonate with Superior Thermostability and Toughness, ACS Appl. Mater. Interfaces 13(25) (2021) 30061-30075. https://doi.org/10.1021/acsami.1c07153.

[52] Q. Chen, S.Q. Huo, Y.X. Lu, M.M. Ding, J.B. Feng, G.B. Huang, H. Xu, Z.Q. Sun, Z.Z. Wang, P.G. Song, Heterostructured Graphene@Silica@Iron Phenylphosphinate for Fire-Retardant, Strong, Thermally Conductive Yet Electrically Insulated Epoxy Nanocomposites, Small 20(31) (2024) 10724. https://doi.org/10.1002/smll.202310724.